sium concentrations (*22*) and reactivity to specific antibodies (*26*), are not shared by U2AF^{65}. Finally, studies reporting protein-protein interactions among SR proteins failed to detect interactions between the U2AF^{65} RS region and other splicing factors (*23*, *27*). Taken together, these observations suggest that there are two distinct classes of RS domains.

The orchestrated formation and disruption of short RNA-RNA helices is a common theme in pre-mRNA splicing (*28*) and probably in other processes that involve RNA. Here we have described a mechanism by which a spliceosomal RNA-RNA base-pairing interaction can be regulated by a protein.

REFERENCES AND NOTES

1. M. J. Moore, C. C. Query, P. A. Sharp, in *The RNA World*, R. F. Gesteland and J. F. Atkins, Eds. (Cold Spring Harbor Laboratory Press, Cold Spring Harbor, NY, 1993), p. 303.
2. R. Parker, P. G. Siciliano, C. Guthrie, *Cell* **49**, 229 (1987); J. Y. Wu and J. L. Manley, *Genes Dev.* **3**, 1553 (1989); Y. Zhuang and A. M. Weiner, *ibid.*, p. 1545.
3. P. E. Hodges and J. D. Beggs, *Curr. Biol.* **4**, 264 (1994).
4. B. Ruskin, P. D. Zamore, M. R. Green, *Cell* **52**, 207 (1988); P. D. Zamore and M. R. Green, *Proc. Natl. Acad. Sci. U.S.A.* **86**, 9243 (1989).
5. P. D. Zamore, J. G. Patton, M. R. Green, *Nature* **355**, 609 (1992).
6. C. G. Burd and G. Dreyfuss, *Science* **265**, 615 (1994).
7. J. Valcárcel, R. Singh, P. D. Zamore, M. R. Green, *Nature* **362**, 171 (1993).
8. R. Singh, J. Valcárcel, M. R. Green, *Science* **268**, 1173 (1995).
9. Modifications in the RS region did not affect binding to the Py tract (*12*) (see also Fig. 2B), as expected from previous studies (*5*, *8*).
10. R. K. Gaur, J. Valcárcel, M. R. Green, *RNA* **1**, 407 (1995).
11. M. J. Moore and P. A. Sharp, *Science* **256**, 992 (1992).
12. J. Valcárcel and M. R. Green, unpublished observations.
13. D. A. Wassarman and J. A. Steitz, *Science* **257**, 1918 (1992).
14. Interestingly, the region in U6 that forms base pairs with U2 is immediately upstream of a pyrimidine stretch [T.-P. Hausner, L. M. Giglio, A. M. Weiner, *Genes Dev.* **4**, 2146 (1990)], suggesting that U2AF^{65} could bind to this sequence to modulate the U2-U6 interaction. Alternatively, this effect could be due to the general annealing activity associated with the U2AF^{65} RS region (*18*).
15. C. C. Query, M. J. Moore, P. A. Sharp, *Genes Dev.* **8**, 587 (1994).
16. Even protein-protein interaction motifs composed predominantly of a single amino acid, such as acidic transcription activation and proline-rich SH3 domains, contain additional types of residues also critical for activity [S. J. Triezenberg, *Curr. Opin. Genet. Dev.* **5**, 190 (1995); T. Pawson and J. Schlessinger, *Curr. Biol.* **3**, 434 (1993)].
17. P. Zuo and J. L. Manley, *Proc. Natl. Acad. Sci. U.S.A.* **91**, 3363 (1994).
18. C.-G. Lee, P. D. Zamore, M. R. Green, J. Hurtwitz, *J. Biol. Chem.* **268**, 13472 (1993).
19. M. R. Green, *Annu. Rev. Genet.* **20**, 671 (1986); C. W. J. Smith and B. Nadal-Ginard, *Cell* **56**, 749 (1989).
20. M. Feughelman *et al.*, *Nature* **175**, 834 (1955).
21. B. Calnan *et al.*, *Science* **252**, 1167 (1991).
22. A. M. Zahler, W. S. Lane, J. A. Stolk, M. B. Roth, *Genes Dev.* **6**, 837 (1992).
23. J. Wu and T. Maniatis, *Cell* **75**, 1061 (1993); J. Kohtz *et al.*, *Nature* **368**, 119 (1994); H. Amrein, M. L. Hedley, T. Maniatis, *Cell* **76**, 735 (1994).
24. P. Zuo and J. L. Manley, *EMBO J.* **12**, 4727 (1993).
25. J. F. Cáceres and A. R. Krainer, *ibid.*, p. 4715.
26. M. B. Roth, A. M. Zahler, J. A. Stolk, *J. Cell Biol.* **115**, 587 (1991).
27. Y. Ono, M. Ohno, Y. Shimura, *Mol. Cell. Biol.* **14**, 7611 (1994); J. Fleckner and M. R. Green, unpublished observations.
28. H. Madhani and C. Guthrie, *Annu. Rev. Genet.* **28**, 1 (1994).
29. Buffer D: 20 mM Hepes (pH 8.0), 0.2 mM EDTA, 20% glycerol, 0.05% NP-40, and 1 mM dithiothreitol.
30. Plasmid pMINX [M. Zillmann *et al.*, *Mol. Cell. Biol.* **8**, 814 (1988)] was used to generate pPy-MINX (pre-mRNA positions 165 to 177 substituted by AUCCAGGAAUUCUAAUACGACUCACUAU) and pbp^m-MINX (pre-mRNA positions 150 to 160 substituted by UAUGAUAGUGA). The corresponding pre-mRNAs were generated by in vitro transcription of Bam HI–digested templates.
31. Plasmids pT7U2 [A. M. Kleinschmidt *et al.*, *Nucleic Acids Res.* **17**, 4817 (1989)], pT7U2ΔBPRS (deletion of U2 snRNA positions 37 to 42), and pHU1A [J. R. Patton, R. J. Patterson, T. Pederson, *Mol. Cell. Biol.* **7**, 4030 (1987)] were used to transcribe U2 snRNA (positions 1 to 71), ΔBPRS, and U1 snRNA, respectively.
32. Abbreviations for the amino acid residues are as follows: A, Ala; C, Cys; D, Asp; E, Glu; F, Phe; G, Gly; H, His; I, Ile; K, Lys; L, Leu; M, Met; N, Asn; P, Pro; Q, Gln; R, Arg; S, Ser; T, Thr; V, Val; W, Trp; and Y, Tyr.
33. RS (U2AF^{35}): positions 561 to 723 of U2AF^{35} cDNA [M. Zhang *et al.*, *Proc. Natl. Acad. Sci. U.S.A.* **89**, 8769 (1992)]. RS (SF2): positions 887 to 1039 of ASF/SF2 cDNA [H. Ge *et al.*, *Cell* **66**, 373 (1991); A. R. Krainer *et al.*, *ibid.*, p. 383].
34. U2AF^{65} Δ(1–55) was prepared by deletion of a Bam HI–Xma I fragment from pGEX3X-U2AF^{65} (*5*) and religation after Klenow treatment. U2AF^{65} Δ(1–63) has been described (*5*). U2AF^{65} Δ(1–94) was prepared by inserting a U2AF^{65} cDNA fragment encoding amino acids 94 to 475, flanked by Bam HI and Eco RI, into the same sites in pGEX-2T [D. B. Smith and K. S. Johnson, *Gene* **67**, 31 (1988)]. Digestion of this construct with Bam HI was used to obtain all the RS mutant derivatives.
35. Inserts were obtained by annealing complementary oligodeoxyribonucleotides corresponding to sequences encoding the RS repeats or mutant derivatives.
36. U2AF^{65} was cloned in plasmid pGEX-CS [T. D. Parks *et al.*, *Anal. Biochem.* **216**, 413 (1994)] to generate a GST-U2AF^{65} fusion with a TEV protease cleavage site between the two polypeptides. The fusion protein was expressed in bacteria, purified, and cleaved with TEV protease as described by Parks *et al.* (*ibid.*).
37. M. Mirfakhrai and A. M. Weiner, *Nucleic Acids Res.* **21**, 3591 (1993).
38. Reactions (20 μl) containing 75% buffer D (*29*), 75 mM KCl, 10 fmol of adenovirus-major-late (AdML) promotor derived pre-mRNAs (*30*), 50 fmol of U2 snRNA, ΔBPRS or U1 snRNA (*31*), recombinant U2AF^{65} or derivatives (50 ng/μl), psoralen (20 μg/ml), and pGEM3 plasmid (47 ng/μl) were irradiated at 25°C with 366-nm ultraviolet light (UVP Inc. lamp, at a distance of 3.5 cm from the samples) for 30 min. Under these conditions, U2AF^{65} promoted interactions between U2 snRNA and a variety of pre-mRNAs from *Drosophila* to human genes.
39. Primer extension mapping of psoralen cross-links has been shown to give rise to more than one primer extension stop from a single cross-link [G. Ericson and P. Wollenzien, *Anal. Biochem.* **174**, 215 (1988); J. Teare and P. Wollenzien, *Nucleic Acids Res.* **18**, 855 (1990)].

40. We thank M. Jacobson and T. Pederson for the U1 snRNA clone, L. Chiang and J. Kielty for technical support, T. O'Toole for secretarial assistance, and F. Gebauer, K. Neugebauer, and members of the Green lab for advice and comments on the manuscript. Supported by European Molecular Biology Organization and Spanish Ministerio de Educación y Ciencia fellowships to J.V., Leukemia Society of America postdoctoral and special fellowships to R.S., and a grant from the National Institutes of Health to M.R.G.

25 June 1996; accepted 30 July 1996

Small-Conductance, Calcium-Activated Potassium Channels from Mammalian Brain

M. Köhler, B. Hirschberg, C. T. Bond, J. M. Kinzie, N. V. Marrion, J. Maylie, J. P. Adelman*

Members of a previously unidentified family of potassium channel subunits were cloned from rat and human brain. The messenger RNAs encoding these subunits were widely expressed in brain with distinct yet overlapping patterns, as well as in several peripheral tissues. Expression of the messenger RNAs in *Xenopus* oocytes resulted in calcium-activated, voltage-independent potassium channels. The channels that formed from the various subunits displayed differential sensitivity to apamin and tubocurare. The distribution, function, and pharmacology of these channels are consistent with the SK class of small-conductance, calcium-activated potassium channels, which contribute to the afterhyperpolarization in central neurons and other cell types.

Action potentials in vertebrate neuronsare followed by an afterhyperpolarization (AHP) that may persist for several seconds and may have profound consequences for the firing pattern of the neuron. The AHP has several components. The fast component (fAHP) helps to repolarize the action potential and regulates spike interval, whereas subsequent slow components (sAHP) underlie spike-frequency adaptation (*1*–*5*).

Each component of the AHP is kinetically distinct and is mediated by different Ca^{2+}-activated K^+ channels. The large-conductance (100 to 200 pS), voltage- and Ca^{2+}-activated K^+ channels (BK channels) underlie the fAHP (*6*, *7*), which develops rapidly (1 to 2 ms) and decays within tens

of milliseconds. The channels underlying the sAHP are SK channels, which differ from BK channels in that they are more Ca^{2+}-sensitive, are activated in a voltage-independent manner, and have a smaller unit conductance (*8*, *9*). The sAHP varies considerably in different cell types, activating slowly (10 to 1000 ms), and it may decay over several seconds (*6*, *9*–*11*).

The fAHP is blocked by low concentrations of external tetraethylammonium and charybdotoxin, in accord with the pharmacology of BK channels (*6*, *7*, *12*). In contrast, the sAHP is insensitive to these agents but exhibits one or the other of two classes of behavior regarding sensitivity to the bee venom peptide toxin apamin. In hippocampal pyramidal neurons the sAHP is insensitive to apamin (*4*), whereas in hippocampal interneurons it is blocked by nanomolar concentrations of the toxin (*13*).

Voltage-independent, apamin-sensitive K^+ channels activated by submicromolar concentrations of Ca^{2+} have been described for peripheral cell types, including skeletal muscle (*14*), gland cells (*15*, *16*), and T lymphocytes (*17*). These channels have unitary conductances of 5 to 20 pS. Apamin-insensitive SK channels have also been reported (*8*). Thus, SK channels make up a subfamily of Ca^{2+}-activated K^+ channels that play key physiological roles in many cell types. We present here the molecular structures for a class of K^+ channel subunits with six transmembrane domains. The characteristics of the expressed channels define this class as SK channels.

A sequence with homology to the pore region of cloned K^+ channels was detected in a database search (*18*) and was used as a probe on cDNA libraries. Three full-length coding sequences were isolated, one from human (hSK1) and two from rat (rSK2, rSK3) brain, and a partial clone, rSK1, representing the rat homolog of hSK1. The sequences predict proteins of 561 (hSK1), 580 (rSK2), and 553 (rSK3) amino acids (Fig. 1A). Hydrophobicity analysis predicts six transmembrane segments with the NH_2- and COOH-termini residing inside the cell (Fig. 1B). The sequences are highly conserved across their transmembrane cores (80 to 90% identity) but diverge in sequence and length within their NH_2- and COOH-terminal domains. The fourth predicted membrane-spanning domain contains three positively charged amino acids, separated by six and seven residues. Multiple consensus targets for phosphorylation by several protein kinases are found in all clones; however, each clone contains potential phosphorylation sites not conserved among all members. There are no conserved N-linked glycosylation sites (NXXS/T) (*19*) in predicted extracellular domains and no consensus nucleotide or Ca^{2+} binding domains (E-F hands). Although related in topology to voltage-dependent K^+ channels, including a P region and S4 segment, the clones reside on a distinct evolutionary branch within the K^+ channel superfamily (Fig. 1C).

Sequences distinct for each of the rat clones were used as probes for in situ hybridizations on sections prepared from rat brain (*20*). The mRNAs are broadly distributed throughout the central nervous system, in characteristic but overlapping patterns (Fig. 2, A through C). The rSK1 and rSK2 probes were also used on Northern (RNA) blots prepared with mRNA isolated from total brain and several peripheral tissues. The rSK1 probe detected mRNAs of different sizes in brain (3.2 kb) and heart (4.4 kb), whereas the rSK2 mRNA was detected in brain and adrenal gland as two bands of 2.2 and 2.4 kb (Fig. 2D) (*21*).

In vitro–synthesized mRNAs were injected into *Xenopus* oocytes, and two-electrode, voltage-clamp recordings were performed 2 to 5 days later (*22*). Voltage protocols failed to evoke currents different

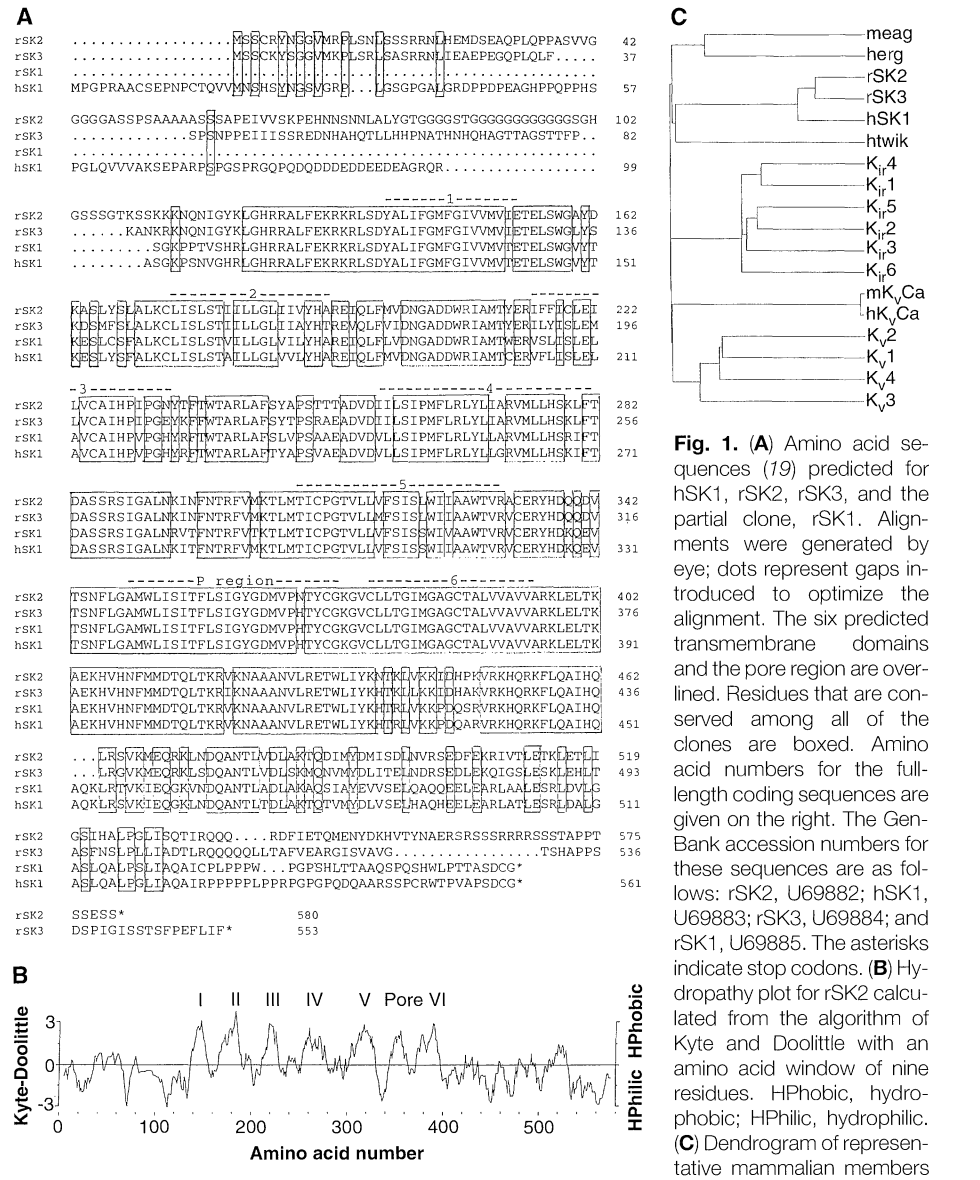

Fig. 1. (**A**) Amino acid sequences (*19*) predicted for hSK1, rSK2, rSK3, and the partial clone, rSK1. Alignments were generated by eye; dots represent gaps introduced to optimize the alignment. The six predicted transmembrane domains and the pore region are overlined. Residues that are conserved among all of the clones are boxed. Amino acid numbers for the full-length coding sequences are given on the right. The GenBank accession numbers for these sequences are as follows: rSK2, U69882; hSK1, U69883; rSK3, U69884; and rSK1, U69885. The asterisks indicate stop codons. (**B**) Hydropathy plot for rSK2 calculated from the algorithm of Kyte and Doolittle with an amino acid window of nine residues. HPhobic, hydrophobic; HPhilic, hydrophilic. (**C**) Dendrogram of representative mammalian members of the K^+ channel superfamily (*18*). The horizontal branch length is inversely proportional to the similarity between sequences.

M. Köhler, B. Hirschberg, C. T. Bond, J. M. Kinzie, N. V. Marrion, J. P. Adelman, Vollum Institute, L-474, Oregon Health Sciences University, 3181 Southwest Sam Jackson Road, Portland, OR 97201, USA.
J. Maylie, Department of Obstetrics and Gynecology, Oregon Health Sciences University, Portland, OR 97201, USA.
*To whom correspondence should be addressed.

from control oocytes. Because of the similar mRNA distribution in brain of rSK2 and mGluR1a, a metabotropic glutamate receptor (*23*, *24*), mGluR1a mRNA was injected with or without the SK mRNAs. The application of glutamate to oocytes expressing only mGluR1a evoked a transient inward current due to activation of endogenous Ca^{2+}-activated Cl^- channels after the release of intracellular Ca^{2+} (Fig. 3A) (*23*, *24*). In oocytes coexpressing mGluR1a with rSK2, application of glutamate evoked the same Cl^- current, which was followed by an outward current (Fig. 3B). Similar results were obtained with rSK3 and hSK1. Intracellular injection of the Ca^{2+} chelator EGTA (~10 mM, final concentration) (*25*) abolished both current responses evoked by subsequent application of glutamate (Fig. 3C), indicating that both components are Ca^{2+}-activated. The ion selectivity of rSK2 was examined in oocytes injected with only the rSK2 mRNA (*26*). The current activated by injection of Ca^{2+} (~1 mM final concentration) reversed near the K^+ reversal potential in ND96 solution. The reversal potential of the currents shifted with increasing extracellular K^+ with a slope of 55.4 mV for a 10-fold change in K^+ concentration (2 to 20 mM K^+, substituted for Na^+), confirming that the channels are selective for K^+ over Na^+.

Macroscopic currents were also recorded

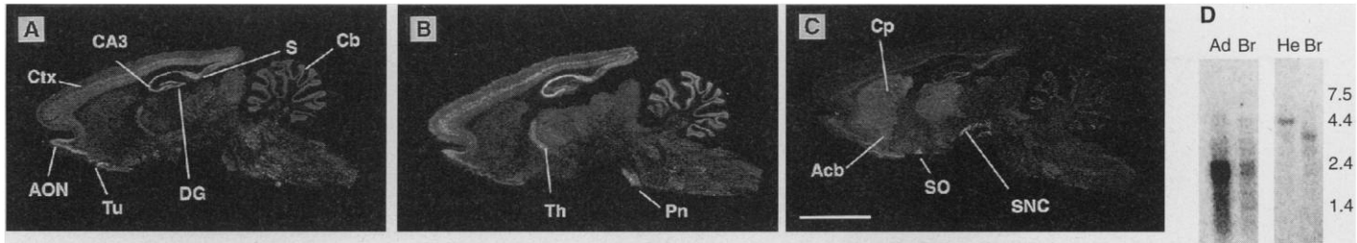

Fig. 2. In situ hybridization and Northern blot analysis for rSK mRNAs. (**A**) Autoradiogram of in situ hybridization with an antisense rSK1 RNA probe. Hybridization was found in the hippocampus (CA3), the dentate gyrus (DG), the subiculum (S), the anterior olfactory nucleus (AON) and olfactory tubercle (Tu), the cerebellum (Cb), and the cortex (Ctx). (**B**) Autoradiogram of in situ hybridization with an antisense rSK2 RNA probe. Of the SK mRNAs, rSK2 mRNA was the most widely expressed and was highest in the hippocampus (not labeled), with lower levels of expression in the olfactory bulb and the anterior olfactory nucleus, the granular layer of the cerebellum (not labeled), the reticular nucleus of the thalamus (Th), and the pontine nucleus (Pn). (**C**) Autoradiogram of in situ hybridization with an antisense rSK3 RNA probe. Hybridization was seen in the lateral septum and ventral tegmental area, the olfactory tubercle (not labeled), the caudate-putamen (Cp), the nucleus accumbens (Acb), the supraoptic nucleus (SO), many nuclei of the thalamus and hypothalamus (not labeled), and the substantia nigra pars compacta (SNC). Scale bar, 5 mm. (**D**) Northern blot analysis of rSK1 and rSK2 mRNAs. Polyadenylated [poly(A)$^+$] mRNA (3 μg) from rat whole brain, heart, lung, spleen, adrenal gland, liver, kidney, and skeletal muscle was prepared as a Northern blot and probed with riboprobes specific for either rSK1 (right) or rSK2 (left); rSK1 mRNA was detected in rat brain (Br) and heart (He), and rSK2 mRNA was detected in brain and adrenal gland (Ad). Neither rSK1 nor rSK2 mRNA was detected from lung, liver, kidney, thymus, spleen, or skeletal muscle. Molecular sizes are indicated in kilobases.

Fig. 3. Expression of rSK2 and hSK1 in *Xenopus* oocytes. In (A) through (C), the metabotropic glutamate (Glut) receptor mGluR1a was expressed with or without rSK2 in *Xenopus* oocytes. Whole cell currents were measured from oocytes superfused with ND96 solution 2 to 3 days after mRNA injection. The holding potential was −80 mV. (**A**) Addition of glutamate (1 mM) to an oocyte injected with mGluR1a mRNA alone evoked a transient Ca^{2+}-activated Cl^- current. Similar results were obtained in six other oocytes injected with mGluR1a. (**B**) Addition of glutamate (1 mM) to oocytes coinjected with mGluR1a and rSK2 mRNA evoked the transient Ca^{2+}-activated Cl^- current observed with mGluR1a-injected oocytes, followed by a large transient outward current. Similar results were obtained in 14 other oocytes coinjected with mGlu1a and rSK2. (**C**) Injection of EGTA (final concentration, ~10 mM) abolished the response to subsequent addition of glutamate in oocytes coinjected with mGluR1a and rSK2 mRNA. Similar results were obtained in three other oocytes coinjected with mGluR1a and rSK2. (**D** and **E**) Currents evoked by voltage steps from inside-out macropatches excised from an oocyte expressing rSK2 (D) or hSK1 (E). With 5 μM Ca^{2+} in the intracellular solution, the membrane was stepped from a holding potential of −80 mV to test potentials between −100 and 100 mV and then repolarized to −50 mV. Currents activated instantaneously and showed no inactivation during the 500-ms test pulses. (**F** and **G**) Current traces (*I*) elicited by 2.5-s voltage ramps (V_m) from −100 to 100 mV from inside-out macropatchs excised from oocytes expressing rSK2 (F) or hSK1 (G). The traces were obtained in the presence of the indicated concentrations of intracellular Ca^{2+}; current amplitudes increased as the Ca^{2+} concentration was increased. (**H** and **I**) The relation between Ca^{2+} concentration and response obtained from the patches shown above for rSK2 (H) or hSK1 (I) channels. The slope conductance, *G*, at the reversal potential is plotted as a function of Ca^{2+} concentration. The data were fitted with the Hill equation, yielding a $K_{0.5}$ of 0.43 μM and 0.71 μM and a Hill coefficient of 4.8 and 3.9 for rSK2 and hSK1, respectively.

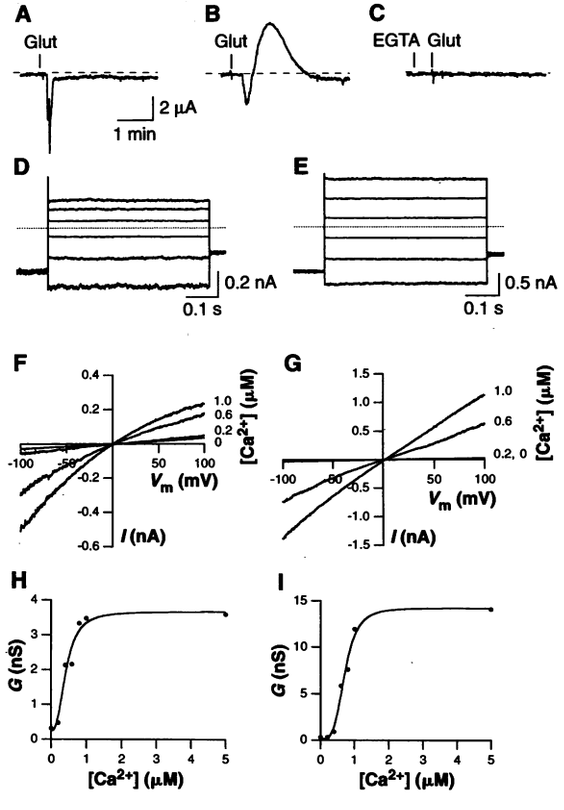

from excised patches (*27*). Application of Ca^{2+} to the cytoplasmic face of inside-out macropatches from oocytes expressing rSK2 or hSK1 evoked substantial currents that were not detected in the absence of Ca^{2+}, nor were they detected from control oocytes. Voltage steps to potentials between −100 and 100 mV evoked time-independent currents (Fig. 3, D and E) that were not obviously voltage-dependent. The Ca^{2+} sensitivity of rSK2 and hSK1 was determined. Currents evoked by voltage ramps from an inside-out macropatch were dependent on the concentration of Ca^{2+} on the intracellular face of the membrane (Fig. 3, F and G). The slope conductance at the reversal potential was plotted as a function of Ca^{2+} concentration, and the data points were fitted with the Hill equation (Fig. 3, H and I). For rSK2 the average $K_{0.5}$ (concentration for half-maximal activation) for Ca^{2+} was 0.63 ± 0.23 μM (n = 8), and for hSK1 it was 0.70 ± 0.06 μM (n = 4). The steep dependence on Ca^{2+} seen from the plots was reflected by a Hill coefficient of 4.81 ± 1.46 for rSK2 and 3.90 ± 0.45 for hSK1, which suggests that at least four Ca^{2+} ions were involved in channel gating. These results identify this family as Ca^{2+}-activated K^+ channels.

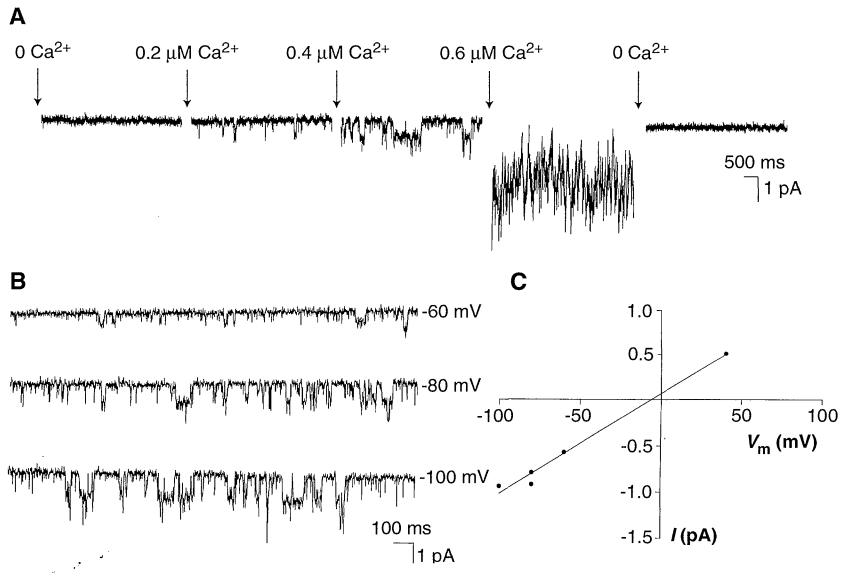

Fig. 4. Single-channel recordings of rSK2. (**A**) Continuous recording at different internal Ca^{2+} concentrations from a representative inside-out patch containing rSK2 channels. Addition of 0.2 μM Ca^{2+} elicited openings to a single amplitude. Increasing Ca^{2+} to 0.4 μM increased channel activity, and openings to several levels are apparent. Upon addition of 0.6 μM Ca^{2+}, channel activity increased such that discrete amplitudes could not be resolved. Channel activity ceased when Ca^{2+} was removed. Gaps represent breaks in the continuously acquired recording. The baseline (zero current level) of the segment recorded in 0.6 μM Ca^{2+} has been aligned by eye. For display, data were digitally filtered at 300 Hz. (**B**) Channel activity from a representative patch recorded in the presence of 0.4 μM Ca^{2+} at −60, −80, and −100 mV. The patch contained more than one channel, and double openings are apparent. For display, traces were digitally filtered at 300 Hz. (**C**) Single-channel current-voltage relation for the patch presented in (B). Data points were derived from the fitting of amplitude histograms at each membrane potential. Linear regression yielded a single-channel conductance of 10.8 pS, with a reversal at −6 mV.

We examined single channels using inside-out patches excised from oocytes expressing rSK2 or hSK1 (*28*). Addition of Ca^{2+} at submicromolar concentrations induced channel activity not seen in controls. The representative patch from an oocyte expressing rSK2 (Fig. 4A) shows that 0.2 μM Ca^{2+} applied to the cytoplasmic side of the patch induced openings to a single amplitude. Channel activity increased as the Ca^{2+} concentration was increased, such that, in 0.6 μM Ca^{2+}, unitary openings could no longer be resolved. Upon washout of Ca^{2+}, channel activity ceased. At 0.4 μM Ca^{2+}, channel open probability was not obviously voltage-dependent, similar to macroscopic ramp recordings (Fig. 4B). Unitary openings measured at several voltages were used to construct a single-channel current-voltage relation (Fig. 4C). Results obtained from three patches yielded a mean single-channel conductance for rSK2 of 9.9 ± 0.9 pS. Similar experiments with hSK1 yielded a single-channel conductance of 9.2 ± 0.3 pS (n = 3).

The functional characteristics of the cloned channels are reminiscent of those of the SK class of Ca^{2+}-activated K^+ channels described in neurons (*6, 8, 29*), skeletal muscle (*14*), adrenal chromaffin cells (*16, 30*), and T lymphocytes (*17*). Native SK channels present a distinct pharmacology. Many but not all SK channels are blocked by apamin and the plant alkyloid, *d*-tubocurare (dTC) (*13, 16, 31*). The rSK2 currents were potently blocked by picomolar concentrations of extracellular apamin with an inhibition constant K_i of 63 pM (Fig. 5, A and B). In contrast, application of 100 nM apamin did not affect hSK1 currents (n = 8). The rSK2 currents were also blocked by extracellular dTC with a K_i of 2.4 μM; hSK1 was ~30-fold less sensitive, with a K_i of 76.2 μM (Fig. 5, C and D).

Activation of SK channels underlies the sAHP in central neurons. Distinguishing features of endogenous SK channels are their activation by submicromolar Ca^{2+}, lack of voltage-dependent gating, and unit conductance (*8, 14, 16*). The sAHP in many neurons is blocked by picomolar concentrations of apamin, whereas in others it is not affected. Cloned members of this family exhibit these features. Indeed, the pattern of in situ hybrid-

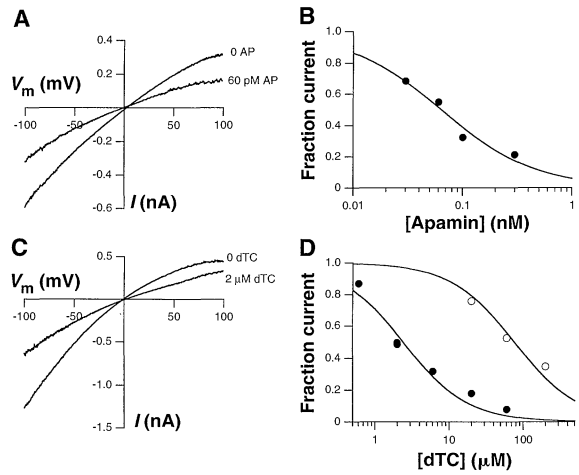

Fig. 5. Pharmacology of rSK2 and hSK1. (**A** and **C**) Macroscopic rSK2 currents were recorded in 5 μM Ca^{2+} from inside-out macropatches with either 0 or 60 pM apamin (AP) (A) or 0 or 2 μM *d*-tubocurare (dTC) (C) in the extracellular solution. (**B** and **D**) Dose-response curves for block by external apamin [shown in (B) for rSK2] or *d*-tubocurare [shown in (D) for rSK2, closed circles, and hSK1, open circles]. Block was determined from multiple inside-out macropatches with or without drug. Each data point represents the fractional current (drug per control) at −100 mV from the average of six control patches and six subsequent patches with drug. Currents were elicited by voltage ramps as in (A). The continuous lines represent nonlinear least squares fits to the data for a 1:1 stoichiometry, giving a K_i of 63 pM for AP and 2.4 μM (rSK1) or 76.2 μM (hSK1) for dTC.

ization for rSK2 mRNA is coincident with the pattern of radiolabeled apamin binding in rat brain (*32*).

The cloned SK subunits contain no significant amino acid homology to other cloned K^+ channel subunits except for a 12-residue stretch within the putative pore domain. Hydrophobicity plots predict that these subunits contain six transmembrane domains, a topology shared with members of the voltage-gated class of K^+ channels (*33*). Like the cyclic nucleotide–gated channels, the cloned SK channels contain an S4 domain with positively charged residues but are not gated in a voltage-dependent manner (*34*). It has been proposed that the charged residues in the S4 segment may form salt bridges with other residues in different regions of the channel, imparting structural stability, even when the charged residues do not participate in voltage sensing (*35*, *36*). In some cells, such as hippocampal pyramidal neurons, the sAHP is regulated by transmitters that act through protein kinases (*8*, *37*). Although it is unclear whether the kinases influence the sAHP through direct phosphorylation of native SK channels or through intermediary effectors, the primary sequences for all of the cloned SK subunits contain many potential phosphorylation sites.

Several hypotheses have been advanced to account for the differences in the sAHP among different cell types (*11*, *29*). The complement of expressed SK subunits, their subcellular distribution, and regulation all may be responsible for differences in the sAHP after an action potential. The shared characteristics of the SK channels responsible for the sAHP were faithfully recapitulated by the clones presented here. The molecular mechanisms underlying variability in sAHPs will likely be understood as this K^+ channel family is further characterized.

REFERENCES AND NOTES

1. J. R. Hotson and D. A. Prince, *J. Neurophysiol.* **43**, 409 (1980).
2. B. Gustaffson and H. Wigstrom, *Brain Res.* **206**, 462 (1981).
3. Y. Yarom, M. Sugimori, R. Ilinas, *Neuroscience* **16**, 719 (1985).
4. B. Lancaster and P. R. Adams, *J. Neurophys.* **55**, 1268 (1986).
5. R. A. Nicoll, *Science* **241**, 545 (1988).
6. B. Lancaster and R. A. Nicoll, *J. Physiol. (London)* **389**, 187 (1987).
7. F. Viana, D. A. Bayliss, A. J. Berger, *J. Neurophysiol.* **69**, 2150 (1993).
8. B. Lancaster, R. A. Nicoll, D. J. Perkel, *J. Neurosci.* **11**, 23 (1991).
9. P. Sah, *J. Neurophysiol.* **74**, 1772 (1995).
10. J. F. Storm, *J. Physiol. (London)* **409**, 171 (1989).
11. B. Lancaster and R. S. Zucker, *ibid.* **475**, 229 (1994).
12. A. Butler, S. Tsunoda, D. P. McCobb, A. Wei, L. Salkoff, *Science* **261**, 221 (1993).
13. L. Zhang and C. J. McBain, *J. Physiol. (London)* **488**, 661 (1995).
14. A. L. Blatz and K. L. Magleby, *Trends Neurosci.* **10**, 463 (1987).
15. A. Tse and B. Hille, *Science* **255**, 462 (1992).
16. Y. B. Park, *J. Physiol. (London)* **481**, 555 (1994).
17. S. Grissmer, R. S. Lewis, M. D. Cahalan, *J. Gen. Physiol.* **99**, 63 (1992).
18. A BLAST search of the expressed sequence tag (EST) database, using the query sequence FXSIPXXXWWAXVTMTTVGYGDMXP (*19*) and allowing for mismatches, retrieved known K^+ channel sequences and GenBank entry M62043. Oligonucleotides corresponding to nucleotides 6 to 36 (sense) and 258 to 287 (antisense) of M62043 were synthesized (Genosys), radiolabeled with polynucleotide kinase (BRL) and ^{32}P-labeled adenosine triphosphate (DuPont Biotechnology Systems), and used to screen ~10^6 recombinant phage from the human hippocampal cDNA library [40% formamide; 1 M NaCl, 1% SDS, 37°C; washed with 1× standard saline citrate (SSC) (150 mM NaCl, 15 mM sodium citrate, pH 7.2) 50°C]. We purified double positively hybridizing phage by rescreening at reduced densities. The cDNA inserts were subcloned into M13, and the nucleotide sequences were determined with T7 DNA polymerase (Sequenase, United States Biochemical). A fragment of this clone containing the pore domain (amino acids 325 to 522) was radiolabeled with random primers (Boehringer) and used to screen a rat brain cDNA library (30% formamide, 1 M NaCl, 1% SDS, 37°C; washed with 2× SSC, 50°C). Positively hybridizing phage were purified and the nucleotide sequences of the inserts determined. We performed computer analyses using the GCG software suite (Genetics Computer Group; version 8.1). We generated the dendrogram using the PILEUP multiple sequence analysis program with full-length coding sequences for the listed subunits. The gap penalty was 3, and the gap extension penalty was 0.5. Specific members of subfamilies, and their accession numbers are as follows: K_v1 ($hK_v1.1$; L02750); K_v2 (mshab; M64228); K_v3 ($mK_v3.3$; X60796); K_v4 (mshal; M64226); $K_{ir}1$ (RomK1; X72341); $K_{ir}2$ (Irk1; X73052) $K_{ir}3$ (Girk1; U01071); $K_{ir}4$ ($K_{ir}4.1$/Bir10; X83585); $K_{ir}5$ ($K_{ir}5.1$/Bir9; X83581); $K_{ir}6$ ($K_{ir}6.1$/uKatp; D42145); hK_vCa (hslo; U11717); and mK_vCa (mslo; L16912).
19. Abbreviations for the amino acid residues are as follows: A, Ala; C, Cys; D, Asp; E, Glu; F, Phe; G, Gly; H, His; I, Ile; K, Lys; L, Leu; M, Met; N, Asn; P, Pro; Q, Gln; R, Arg; S, Ser; T, Thr; V, Val; W, Trp; Y, Tyr, and X, unknown.
20. Care and handling of adult female Sprague-Dawley rats were in accordance with institutional guidelines. Rats were deeply anesthetized with pentobarbital and perfused transcardially with ice-cold saline and then with ice-cold 4% paraformaldehyde in 0.1 M sodium borate (pH 9.5). The brains were removed quickly and fixed overnight at 4°C in 4% paraformaldehyde in borate buffer (pH 9.5) containing 10% sucrose. Cryostat microtome sections (25 μm) were mounted onto gelatin- and poly-L-lysine–coated glass slides and incubated for 15 min in 4% paraformaldehyde in 0.1 M phosphate-buffered saline (PBS), washed twice in 0.1 M PBS, and treated for 30 min at 37°C in proteinase K (10 mg/ml) in 100 mM tris, 50 mM EDTA (pH 8) and then with 0.0025% acetic anhydride (w/w) in 0.1 M triethanolamine at room temperature. The sections were then washed in 2× SSC, dehydrated in increasing concentrations of ethanol, and vacuum-dried at room temperature. Templates for probe synthesis represented sequences unique to each of the clones. ^{35}S-labeled antisense cRNA probe was heated to 65°C for 5 min and diluted to 10^7 cpm/ml in hybridization buffer: 66% formamide, 260 mM NaCl, 1.3× Denhardt solution (13 mM tris, pH 8.0, 1.3 mM EDTA, 13% dextran sulfate). Sections in the hybridization mixture were covered with siliconized glass cover slips and sealed with DPX mountant. After the slides had been incubated at 58°C for 20 hours, they were soaked in 4× SSC to remove cover slips, then rinsed in 4× SSC (four times, 5 min each) before treatment with ribonuclease A (20 mg/ml for 30 min at 37°C). The slides were then rinsed in decreasing concentrations of SSC containing 1 mM dithiothreiotol (DTT) to a final stringency of 0.1× SSC, 1 mM DTT for 30 min at 65°C. After the sections had been dehydrated in increasing concentrations of ethanol, they were vacuum-dried and exposed to DuPont Cronex-4 x-ray film for 7 days. The film was scanned by a Microtek ScanMaker 1850S at a resolution of 728 pixels per centimeter, and the images were analyzed with Image v1.55 software (NIH) and Photoshop (Adobe).
21. Total RNA was extracted [J. M. Chirgwin, A. E. Przybyla, R. J. MacDonald, W. J. Rutter, *Biochemistry* **18**, 5294 (1979)] from rat brain, adrenal gland, thymus, spleen, skeletal muscle, heart, kidney, liver, and lung of 3-week-old Sprague-Dawley rats. Polyadenylated [poly(A)$^+$] mRNA was purified by oligo d(T) cellulose chromatography (Collaborative Research), and 3 μg from each tissue was prepared as a Northern blot by electrophoresis through a 1% agarose-formaldehyde gel and transfer to Genescreen (DuPont Biotechnology Systems) nylon membranes. Antisense riboprobes were synthesized from linearized DNA templates with ^{32}P-labeled uridine triphosphate (DuPont Biotechnology Systems). Blots were hybridized in 50% formamide, 5% SDS, 400 mM $NaPO_4$ (pH 7.2), 1 mM EDTA at 60°C for 12 hours; then they were washed in 0.05× SSC at 65°C and visualized with a PhosphorImager 445 SI (Molecular Dynamics) after 15 hours.
22. In vitro mRNA synthesis and oocyte injections were performed as described in [J. P. Adelman *et al.*, *Neuron* **9**, 209 (1992)]. *Xenopus* care and handling were in accordance with institutional guidelines. Frogs underwent no more than two surgeries, separated by at least 3 weeks, and well-established techniques were used for the surgeries. Frogs were anesthetized with an aerated solution of the ethyl ester of 3-aminobenzoic acid. Oocytes were studied 2 to 5 days after injection with 2 ng of mRNA. We measured whole cell currents using a two-electrode voltage clamp with a CA-1 amplifier interfaced to a Macintosh Quadra 650 computer. Data were simultaneously acquired through Pulse (Heka Electronik) at 500 Hz and Chart (AD Instruments) at 10 Hz. During recording, oocytes were continuously superfused with ND96 solution containing 96 mM NaCl, 2 mM KCl, 1.8 mM $CaCl_2$, 1 mM $MgCl_2$, 5 mM Hepes (pH 7.5 with NaOH) at room temperature. To minimize Cl^- currents, some oocytes were soaked and studied in Cl^--free ND96 solution (96 mM sodium gluconate, 2 mM potassium gluconate, 2.7 mM calcium gluconate, 1-mM magnesium gluconate, 5 mM Hepes, pH 7.5 with NaOH).
23. K. M. Houamed *et al.*, *Science* **349**, 760 (1991).
24. M. Masu, Y. Tanabe, K. Tsuchida, R. Shigemoto, S. Nakanishi, *Nature* **349**, 760 (1991).
25. After establishment of the two-electrode voltage clamp, the oocyte was impaled with a third electrode containing 200 mM EGTA, pH adjusted to 7.2 with KOH. We monitored the input resistance during impalement to ensure oocyte viability. At the indicated time, 50 nl of the EGTA solution was injected into the oocyte. If we assume an oocyte volume of 1 μl, the predicted final concentration of EGTA was 10 mM.
26. Two days after injection, the oocytes were soaked for >24 hours in Cl^--free ND96 solution to minimize Cl^- currents. In the two-electrode recording mode, currents were activated by injection of 5 nl of 200 mM $CaCl_2$ through a third electrode, resulting in a final intracellular concentration of ~1 mM Ca^{2+}. This procedure resulted in a longer lasting activation of the K^+ current than that activated by glutamate in oocytes coinjected with mGluR1a and rSK2.
27. Oocytes were injected as described for two-electrode, voltage-clamp recordings. At 2 to 9 days after injection, inside-out macropatches were excised into an intracellular solution containing 116 mM potassium gluconate, 4 mM KCl, 10 mM Hepes (pH 7.25, adjusted with KOH) supplemented with $CaCl_2$ or EGTA or both. To obtain nominally Ca^{2+}-free solution, we added 1 mM EGTA. Alternatively, $CaCl_2$ was added to the cytoplasmic solution to give free Ca^{2+} concentrations (1 to 10 μM). In this case, the proportion of Ca^{2+} binding to gluconate was determined by a computer program (CaBuf) (we used a stability constant for calcium gluconate of 15.9 M^{-1}) [R. M. C. Dawson, D. C. Elliot, W. H. Elliot, K. M. Jones, *Data for Biochemical Research* (Oxford Univ. Press, New York, 1969)]. To obtain Ca^{2+} concentra-

tions below 1 μM, we added 5 mM EGTA to the cytoplasmic solution and added $CaCl_2$ as calculated using the CaBuf program and published stability constants [A. Fabiato and F. Fabiato, *J. Physiol. (London)* **75**, 463 (1979)]. For experiments in which Mg^{2+} was added to the cytoplasmic solution, $MgCl_2$ was added to the total concentrations stated in the text. Under these conditions, binding of Mg^{2+} to gluconate is negligible (stability constant, 1.7 M^{-1}). Electrodes were pulled from thin-walled, filamented borosilicate glass (World Precision Instruments) and filled with 116 mM potassium gluconate, 4 mM KCl, 10 mM Hepes (pH 7.25). Electrode resistance was typically 2 to 5 megohms. Membrane patches were voltage-clamped with an Axopatch 200A amplifier (Axon Instruments). The data were low-pass–Bessel filtered at 2 kHz and were acquired with Pulse software (Heka Electronik). In the analysis we used Pulse, Kaleidograph (Abelbeck), or IGOR (Wavemetrics) software. All experiments were performed at room temperature from a holding potential of −80 mV. Voltage ramps (2.5 s) from −100 to 100 mV were acquired at a sampling frequency of 500 Hz. The currents recorded from macropatches showed small inward rectification in the absence of cytoplasmic cations other than K^+ and Ca^{2+} (5 μM). In the hippocampus, SK channels exhibit significant inward rectification in the presence of intracellular Mg^{2+} (*8*). When different concentrations of Mg^{2+} (0.1 to 3 mM) were added to the intracellular face of inside-out patches, outward currents were reduced. Apamin was from Calbiochem, and *d*-tubocurare was from Research Biochemicals International.

28. Solutions used were the same as for macropatch recordings. Electrodes were pulled from Corning 7052 glass (Garner) and had resistances of 9 to 13 megohms. Data were filtered at 1 kHz (Bessel), acquired at 10 kHz with Pulse (Heka Electronik), and stored directly on a Macintosh Quadra 650. Single channels were analyzed with MacTac (SKALAR Instruments). The "50% threshold" technique was used to estimate event amplitudes. The threshold was adjusted for each opening, and each transition was inspected visually before being accepted. Amplitude histograms were constructed using MacTacfit (SKALAR Instruments), and the single channel conductance was determined from a Gaussian distribution. Channel open probability was estimated from *NP*(o), the product of the open probability multiplied by the number of channels; *NP*(o) was calculated as the sum of the (dwell time multiplied by level number) divided by the total time, and *N* was estimated as the number of simultaneously open channels at 0.4 μM Ca^{2+}.

29. P. Sah and E. M. McLachlan, *J. Neurophysiol.* **68**, 1834 (1992).
30. A. R. Artalejo, A. G. Garcia, E. Neher, *Pfluegers Arch.* **423**, 97 (1993).
31. N. J. Dun, Z. G. Jiang, N. Mo, *J. Physiol. (London)* **375**, 499 (1986).
32. D. R. Gelhert, *Neuroscience* **52**, 191 (1993).
33. L. Y. Jan and Y. N. Jan, *Nature* **345**, 672 (1990).
34. E. H. Goulding, G. R. Tibbs, S. A. Siegelbaum, *ibid.* **372**, 369 (1994).
35. S. R. Durell and H. R. Guy, *Biophys. J.* **62**, 238 (1992).
36. D. M. Papazian *et al.*, *Neuron* **14**, 1293 (1995).
37. P. Pedarzani and J. F. Storm, *Pfluegers Arch.* **431**, 723 (1996).

38. We thank M. Litt for assistance with database searches, J. Saugstad and G. Westbrook for early experiments with mGluR1a, and B. Bean for helpful and enthusiastic discussions. We thank G. Westbrook for supplying the mGluR1a clone and C. Miller for supplying the charybdotoxin. M.K. was supported by a grant from the DRG, B.H. by an NIH cardiology training grant, and J.M.K. by a National Research Service Award grant. This work was supported by NIH grants to J.M. and J.P.A.

2 May 1996; accepted 29 July 1996

A Cyclin-Dependent Kinase–Activating Kinase (CAK) in Budding Yeast Unrelated to Vertebrate CAK

F. Hernan Espinoza, Alison Farrell, Hediye Erdjument-Bromage, Paul Tempst, David O. Morgan*

Progress through the cell cycle is governed by the cyclin-dependent kinases (CDKs), the activation of which requires phosphorylation by the CDK-activating kinase (CAK). In vertebrates, CAK is a trimeric enzyme containing CDK7, cyclin H, and MAT1. CAK from the budding yeast *Saccharomyces cerevisiae* was identified as an unusual 44-kilodalton protein kinase, Cak1, that is only distantly related to CDKs. Cak1 accounted for most CAK activity in yeast cell lysates, and its activity was constant throughout the cell cycle. The *CAK1* gene was essential for cell viability. Thus, the major CAK in *S. cerevisiae* is distinct from the vertebrate enzyme, suggesting that budding yeast and vertebrates may have evolved different mechanisms of CDK activation.

The activation of CDKs requires association with a cyclin subunit and phosphorylation by CAK at a conserved threonine residue (*1*). The major CAK activity in vertebrate and starfish cells is a heterotrimer composed of CDK7, cyclin H, and MAT1 (*2*–*4*). The homologous CDK-cyclin complex in fission yeast also has CAK activity (*5*). However, in the budding yeast *Saccharomyces cerevisiae*, the closest CDK7 homolog (Kin28) does not have CAK activity (*6*, *7*), and the enzyme responsible for CDK activation in this organism is unknown.

To explore the nature of CAK in budding yeast, we used conventional chromatographic methods to purify the major CAK activity in yeast lysates (Fig. 1). We measured CAK activity by testing the ability of column fractions to activate the histone H1 kinase activity of purified human CDK2–cyclin A complexes, which are more readily prepared in large quantities than are yeast Cdc28-cyclin complexes. Peak fractions also activated Cdc28-Clb2 (*8*). We estimate that CAK activity was purified over 1000-fold after six chromatographic steps. In the last steps of purification, CAK activity comigrated with a single protein of ~44 kD on polyacrylamide gels (p44) (Fig. 1, B and C). We were unable to purify p44 to homogeneity; however, in multiple preparations, p44 was the only protein that consistently copurified with CAK activity, suggesting that p44 alone was responsible for the activity. This conclusion is supported by results from gel filtration analysis of CAK activity in crude yeast lysates (*8*) or partially purified CAK preparations (Fig. 1A), in which the apparent molecular size of native CAK was ~45 kD.

Tryptic peptides from p44 were subjected to mass spectrometry and amino acid sequencing. Comparison of peptide sequences with the *Saccharomyces* Genomic Database (Stanford University) revealed that the amino acid sequences of two peptides matched predicted sequences in a previously uncharacterized open reading frame, YFL029c, on chromosome VI (*9*). In addition, the masses of these two peptides, as well as those of two additional peptides from p44, matched the theoretical masses of tryptic peptides in the predicted sequence of YFL029c (Fig. 2). The YFL029c open reading frame encodes a protein with sequence similarity to protein kinases and a molecular size of 42,183 daltons. We conclude that this open reading frame encodes p44, which we call Cak1.

Cak1 is only distantly related to other protein kinases. Its closest known relative in any species is yeast Cdc28, with which it shares limited similarity (~23% identity) (Fig. 2). It is even less similar to yeast Kin28 (17% identity) and is therefore not closely related to the CDK7 subfamily. Cak1 is also distinct from most other protein kinases in that it lacks a highly conserved NH_2-terminal cluster of glycine residues that contributes to the adenosine triphosphate (ATP) binding site (*10*). Cak1 has large amino acid inserts between conserved kinase subdomains. On the basis of studies of protein kinase structure (*11*, *12*), we predict that these inserts are located in loops between conserved secondary

F. H. Espinoza, A. Farrell, D. O. Morgan, Department of Physiology and Department of Biochemistry and Biophysics, University of California, San Francisco, CA 94143–0444, USA.
H. Erdjument-Bromage and P. Tempst, Molecular Biology Program, Memorial Sloan-Kettering Cancer Center, New York, NY 10021, USA.
*To whom correspondence should be addressed.